

Neutrino flavor mixing with moments

McKenzie Myers,¹ Theo Cooper,¹ MacKenzie Warren,² Jim Kneller,^{1,*}
Gail McLaughlin,¹ Sherwood Richers,^{3,†} Evan Grohs,¹ and Carla Fröhlich¹

¹*Department of Physics, North Carolina State University, Raleigh, NC 27695, USA*

²*AI Research Group, 5x5 Technologies, St Petersburg, FL 33701, USA*

³*Department of Physics, University of California Berkeley, Berkeley, CA 94720*

(Dated: November 30, 2021)

The successful transition from core-collapse supernova simulations using classical neutrino transport to simulations using quantum neutrino transport will require the development of methods for calculating neutrino flavor transformations that mitigate the computational expense. One potential approach is the use of angular moments of the neutrino field, which has the added appeal that there already exist simulation codes which make use of moments for classical neutrino transport. Evolution equations for quantum moments based on the quantum kinetic equations can be straightforwardly generalized from the evolution of classical moments based on the Boltzmann equation. We present an efficient implementation of neutrino transformation using quantum angular moments in the free streaming, spherically symmetric bulb model. We compare the results against analytic solutions and the results from more exact multi-angle neutrino flavor evolution calculations. We find that our moment-based methods employing scalar closures predict, with good accuracy, the onset of collective flavor transformations seen in the multi-angle results. However, they over-estimate the coherence between neutrinos traveling along different trajectories in tests that neglect neutrino-neutrino interactions. More sophisticated quantum closures may improve the agreement between the inexpensive moment-based methods and the multi-angle approach.

I. INTRODUCTION

The importance of neutrinos to the core-collapse supernova (CCSN) paradigm has been recognized since the earliest simulations of the explosions by Colgate and White [1]. Even though many details have changed over the years since that pioneering study, neutrinos are still thought to be the driver of the explosions of stars with initial masses $\gtrsim 10 M_{\odot}$ that have reached the end of their nuclear burning lifetimes (see [2–7] for reviews).

Although a complete theoretical accounting of the explosion dynamics remains elusive, state of the art numerical simulations performed in three dimensions appear to be converging toward exploding solutions [8–16]. However, there are still many uncertainties underlying these models. The structure of the progenitor stars is presently poorly understood and is complicated by variations in stellar mass, metallicity, rotation history, magnetic fields, and binary interactions. Another source of uncertainty in the details of the explosion arises from the unknown equation of state describing matter above nuclear densities. Variations in the equation of state have been shown to lead to significant differences in the outcomes of simulations [17–19]. Furthermore, there is yet work to be done to ensure that multidimensional simulations are performed with sufficient resolution and that the approximations employed in various methods (especially regarding neutrino transport) do not significantly affect the solution [20, 21], though there currently seems

to be more agreement than disagreement between full supernova simulation codes [22, 23].

While the recent progress in supernova simulations is impressive, the simulations neglect the quantum nature of the neutrino and its ability to change flavor (though see [24, 25] for some attempts at effective treatments). Until recently, this omission was not thought to be important for the dynamics of the explosion (see [26, 27] for recent reviews). Flavor transformation calculations based on post-processing results from simulations that employ classical transport reveal a number of neutrino flavor oscillation phenomena. As in the Sun, neutrinos undergo complete flavor transformation at a Mikheyev-Smirnov-Wolfenstein (MSW) resonance [28–30] due to the combination of differing neutrino masses and a potential from neutrinos interacting with the background matter. However, this flavor transformation occurs well beyond any supernova engine or nucleosynthesis region and is mostly important for understanding future neutrino detections at Earth, e.g. [31–33]. The neutrino self-interaction potential due to neutrinos interacting with other nearby neutrinos makes the flavor transformation nonlinear. The so-called collective neutrino oscillations, which result from the combined effects of the self-interaction potential and the differing neutrino masses, are also thought to occur too far out to affect the supernova engine in a significant way [24, 34, 35], unless beyond the standard model interactions are included, e.g. [36].

More recently, the so-called fast flavor instability was shown to have the potential to drive significant and rapid flavor transformations well inside the shock if the neutrino distribution fulfils the criterion of an electron lepton number crossing [37–48]. Conditions fulfilling this

* jim_kneller@ncsu.edu

† NSF Astronomy & Astrophysics Postdoctoral Fellow

instability criterion have been shown to exist both inside [49–52] and outside [53] the shock front in simulations that use classical transport. Recent consideration of effects of small-scale turbulence could make the fast flavor instability even more ubiquitous than the electron lepton number crossing criterion predicts [54–56]. Thus these more recent studies now strongly indicate that flavor transformation may occur in regions of the supernova where there could be feedback into the hydrodynamics. While simulations that adopt effective treatments of flavor transformation within the framework of classical neutrino transport may be able to capture such physics in an approximate way, direct calculations of quantum neutrino transport are needed to understand the microscopic instabilities from first principles.

There are several challenges to be overcome in implementing and simulating quantum neutrino transport. One unavoidable consequence is a huge increase in the dynamical range of lengthscales that need to be resolved. At the present time, the spatial resolution of the state-of-the-art simulations approaches lengthscales of order ~ 100 m for a simulation covering a domain size of order ~ 1000 km (i.e a dynamical range of 30 - 40 dB). However, the lengthscale of neutrino flavor oscillations in matter with a density of $\sim 10^{12}$ g/cm³ is of order ~ 1 μ m, which means one would need to simulate a dynamical range of at least ~ 120 dB. Multi-angle collective flavor transformation calculations also require hundreds to thousands of both energy and angle bins in order for the results to converge, far more than the ~ 20 energy bins and ~ 10 angle bins used in simulations of classical transport [21, 57–59]. Thus the computational expense of even a 1D, spherically symmetric supernova simulation using quantum transport is expected to be many orders of magnitude greater than for a simulation using classical transport. One must seriously consider alternative approaches that mitigate this expense if quantum supernova simulations are to be feasible.

One approach, which we consider here, is to use angular moments of the quantum neutrino distribution i.e. quantum moments. Neutrino transport based on angular moments of the classical neutrino radiation field are already used in many state of the art supernova simulation codes due to their computational efficiency (e.g ., [60–65]). Including the quantum kinetic equations describing the evolution of the quantum moments will rely on techniques developed both in the neutrino oscillation literature and in the neutrino transport literature. Vlasenko *et al.* [66] and Volpe [67] developed the equations from first principles, while Blaschke and Cirigliano [68] expressed the collision integral in detail. Investigations of the feasibility of the quantum moment approach have already been taken. Strack and Burrows [69] (see also Duan and Shalgar [70]) outlined a moment-based formalism for the QKEs and Richers *et al.* [71] fleshed out the form of the collision integral using interaction rates in the form commonly used in the core-collapse supernova simulation literature. Richers *et al.* [71] also developed

a code to simulate the QKEs under the assumption of isotropy and homogeneity, and Johns *et al.* [72] used a moment method to analyze the presence of fast flavor instability in parameterized cases.

The goal of this paper is to present results from a new code that solves the quantum moment evolution equations in various scenarios. In Section II we present the quantum kinetic moment equations we use, introduce the one-moment and two-moment schemes and explain the closures we adopt for them. In Section III we investigate how well moment methods are able to produce MSW, and collective oscillations by comparing their results to multi-angle calculations. Finally, we conclude in Section IV and discuss the issues our study uncovers.

II. FLAVOR MIXING WITH MOMENTS

Classical radiation transport is described in general by the Boltzmann equation, but the six-dimensional distribution function is exceedingly expensive to evolve. A moment approach to radiation transport involves taking angular moments of the full Boltzmann equation and evolving a subset of these moments rather than directly discretizing the neutrino distribution in angle. The result is a system of coupled differential equations for a handful of four-dimensional (three spatial and one energy dimension) variables, rather than a differential equation for a six-dimensional distribution function. The angular moments which are evolved or prescribed in a two-moment method in flat spacetime are the differential energy density, (energy) flux vector, and pressure tensor, defined as

$$E(t, \vec{r}, q) = \frac{1}{4\pi} \left(\frac{q}{2\pi\hbar c} \right)^3 \int d\Omega_p f(t, \vec{r}, \vec{p}) \quad (1)$$

$$\vec{F}(t, \vec{r}, q) = \frac{1}{4\pi} \left(\frac{q}{2\pi\hbar c} \right)^3 \int d\Omega_p \hat{p} f(t, \vec{r}, \vec{p}) \quad (2)$$

$$P(t, \vec{r}, q) = \frac{1}{4\pi} \left(\frac{q}{2\pi\hbar c} \right)^3 \int d\Omega_p \hat{p} \otimes \hat{p} f(t, \vec{r}, \vec{p}) , \quad (3)$$

where $q = |\vec{p}|c$. Note that we omit the speed of light from the definition of the flux moment in order that the moments all have the same units. The factor of $1/4\pi$ in each definition of the moments is a units choice made to divide out the 4π from the solid angle integral when tracking the evolution of these variables. This means, the total neutrino flux $\vec{\mathcal{F}}$ is 4π times the integral of the spectral flux

$$\vec{\mathcal{F}} = 4\pi \int_0^\infty \vec{F} dq . \quad (4)$$

The moments for the antineutrinos are defined similarly and shall be denoted with overbars i.e. \bar{E} , $\vec{\bar{F}}$ and \bar{P} . In classical transport f and \bar{f} are distribution functions, taking on values $f \in [0, 1]$ and describing the occupation number per unit of phase space. To generalize so as to

permit flavor mixing, we refine f and \bar{f} to become matrices in flavor space. Thus, the moments also become matrices and the energy density, for example, is now (assuming two neutrino flavors) [69]

$$E(t, \vec{r}, q) \rightarrow \begin{pmatrix} E^{(ee)}(t, \vec{r}, q) & E^{(ex)}(t, \vec{r}, q) \\ E^{(xe)}(t, \vec{r}, q) & E^{(xx)}(t, \vec{r}, q) \end{pmatrix}. \quad (5)$$

The other moments have a similar structure. We shall refer to moments that are matrices in flavor space as ‘quantum moments’ in order to distinguish them from the scalar ‘classical’ definition of moments, and indicate flavor elements of the quantum moments with superscripts in parentheses to avoid confusions with exponents. $E^{(ee)}$ and $E^{(xx)}$ are real, positive definite quantities that represent the differential energy densities in the electron and representative heavy lepton (“ x ”) flavor neutrinos. The off-diagonal components $E^{(ex)}$ and $E^{(xe)}$ represent the flavor overlap and are complex quantities. The luminosity matrices of neutrinos and antineutrinos are calculated

from the radial component F_r and \bar{F}_r of the flux vectors for the neutrinos and antineutrinos respectively, and are

$$L = (4\pi r)^2 c \int F_r dq, \quad (6)$$

$$\bar{L} = (4\pi r)^2 c \int \bar{F}_r dq. \quad (7)$$

Similarly to the quantum moments for the energy density, flux and pressure, the diagonal elements of the luminosity matrices are the luminosities of each neutrino flavor.

The evolution equations for the moments are found by following the procedure outlined in Strack and Burrows [69] and Zhang and Burrows [73] (although the collision terms therein need to be modified as in [68, 71]). There are an infinite number of angular moments and corresponding evolution equations (e.g. [74]). Under the assumption of flat spacetime and spherical symmetry, the evolution equations for the lowest-order moments (energy density and energy flux) take the form

$$\frac{1}{c} \frac{\partial E}{\partial t} + \frac{\partial F_r}{\partial r} + \frac{2F_r}{r} = -\frac{i}{\hbar c} [H_V + H_M + H_E, E] - \frac{i}{\hbar c} [H_F, F_r] + C_E \quad (8)$$

$$\frac{1}{c} \frac{\partial \bar{E}}{\partial t} + \frac{\partial \bar{F}_r}{\partial r} + \frac{2\bar{F}_r}{r} = -\frac{i}{\hbar c} [H_V - H_M - H_E^*, \bar{E}] + \frac{i}{\hbar c} [H_F^*, \bar{F}_r] + \bar{C}_E \quad (9)$$

$$\frac{1}{c} \frac{\partial F_r}{\partial t} + \frac{\partial P_{rr}}{\partial r} + \frac{3P_{rr} - E}{r} = -\frac{i}{\hbar c} [H_V + H_M + H_E, F_r] - \frac{i}{\hbar c} [H_F, P_{rr}] + C_F \quad (10)$$

$$\frac{1}{c} \frac{\partial \bar{F}_r}{\partial t} + \frac{\partial \bar{P}_{rr}}{\partial r} + \frac{3\bar{P}_{rr} - \bar{E}}{r} = -\frac{i}{\hbar c} [H_V - H_M - H_E^*, \bar{F}_r] + \frac{i}{\hbar c} [H_F^*, \bar{P}_{rr}] + \bar{C}_F \quad (11)$$

where we have defined

$$H_E = 4\pi \sqrt{2} G_F \int \frac{dq}{q} (E(q) - \bar{E}^*(q)) \quad (12)$$

$$H_F = -4\pi \sqrt{2} G_F \int \frac{dq}{q} (F_r(q) - \bar{F}_r^*(q)) \quad (13)$$

and * indicates the complex conjugate. Together H_E and H_F are the self-interaction Hamiltonian $H_{SI} = H_E + H_F$. The four terms C_E , \bar{C}_E , C_F and \bar{C}_F are the ‘collision’ terms and in the context of flavor mixing, are also matrices [68, 71]. We neglect the collision terms in the rest of this work. For two flavor mixing, the vacuum Hamiltonian has the form

$$H_V = \frac{\Delta m_{12}^2 c^4}{4q} [\sin(2\theta_{12}) \sigma_1 - \cos(2\theta_{12}) \sigma_3], \quad (14)$$

where $\Delta m_{12}^2 = m_2^2 - m_1^2$ is the splitting between the neutrino masses and θ_{12} is the neutrino vacuum mixing angle. The matter Hamiltonian has the form

$$H_M = \frac{\sqrt{2} G_F n_e}{2} \sigma_3, \quad (15)$$

where n_e is the number density of electrons. In both cases, σ_i is the i ’th Pauli matrix and we have removed terms that contribute only to the trace of the Hamiltonian, as they do not affect the flavor evolution.

A. Neutrino Bulb Model

Our test cases focus upon the inhomogeneous environment around a spherical source of neutrinos i.e. a neutrino bulb. Since this environment has been studied extensively due to its similarity to core-collapse supernovae, we can take advantage of results from other codes which have been developed for this scenario. In what follows we compare our results with the steady-state ‘multi-angle’ BULB model calculations using the SQA code, which is briefly described in Appendix A.

Inspection of Eqns. 8 to 11 reveals that they contain, in general, one more free variable than the number of equations. To avoid an endless tower of equations, we need to close the listed equations by divining a relationship between the moments in those equations. In previous studies of classical moment transport, closures have

been supplied from analytic physical approximations or ad-hoc prescriptions (see [75, 76] for summaries) or characteristic methods (e.g., [77, 78]). There is a wealth of physics buried in the choice of closure and any results will depend on this choice. We leave exploration of the sensitivity to the closure to future work and use here two geometrically motivated examples.

The geometry of the scenario we are considering is shown in Figure 1. At a given radial location r above the source, the neutrinos are confined to propagate within a cone around the radial direction. Neutrinos which are propagating along a trajectory which makes an angle θ with the radial direction have traveled a distance

$$\lambda = r \cos \theta - \sqrt{R_\nu^2 - r^2 \sin^2 \theta} \quad (16)$$

from the neutrinosphere. The half opening-angle of the cone containing all the neutrino trajectories passing through the point of interest is θ_{\max} and from the geometry this angle is found to be

$$\cos \theta_{\max} = \sqrt{1 - (R_\nu/r)^2}. \quad (17)$$

We will use this to self-consistently inform our choice of closures.

1. One-moment closure

The first closure is a relationship between the energy and the radial component of the flux for use in one moment calculations. In classical flux-limited diffusion, the system is similarly closed so as to directly evolve only one moment, though the specific closure is different from that employed here. When the neutrinos are emitted half-isotropically from a spherical bulb and do not oscillate, the integrals defining the scalar energy density and

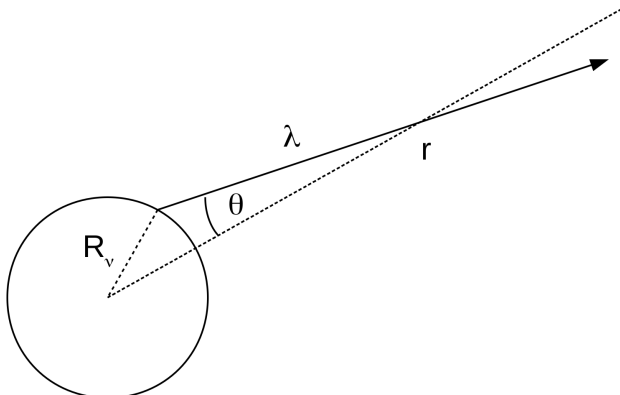


FIG. 1. The bulb model: at a distance r from the center of a opaque neutrino bulb of radius R_ν , the neutrino has traveled a distance λ and its trajectory makes an angle θ with the radial direction.

radial flux (or more generally, the traces thereof) are related analytically. In this case we find the flux is related to the energy density via

$$F_r = \frac{(1 - \cos^2 \theta_{\max})}{2(1 - \cos \theta_{\max})} E. \quad (18)$$

Using Equation 17, this can be used to define a closure as

$$F_r = \frac{E}{2} \left(1 + \sqrt{1 - \left(\frac{R_\nu}{r} \right)^2} \right). \quad (19)$$

In what follows we will refer to this relationship as the “one-moment” closure. Substituting the one-moment closure of Eq. 19 into Eq. 8 gives an equation that is now only a function of the two energy densities. Using this closure, the form of the self-interaction Hamiltonian matches that in the single-angle approximation of Dasgupta *et al.* [79], although we stress that the advection terms in the one-moment approximation differ from those in the single-angle approximation.

2. Two moment closure

In the two moment approximation we simultaneously solve for the evolution of the first two moments as is done in M1 neutrino transport methods common in CCSN modeling. These moments, the energy density E and flux F_j , must be related to the next highest moment, the pressure tensor P_{ij} . In the neutrino bulb model, in the absence of oscillations, we find that the rr -component of the pressure tensor can be related to the energy density via

$$P_{rr} = \frac{(1 - \cos^3 \theta_{\max})}{3(1 - \cos \theta_{\max})} E. \quad (20)$$

Using Equation 17, this becomes

$$P_{rr} = \left(2 - \left(\frac{R_\nu}{r} \right)^2 + \sqrt{1 - \left(\frac{R_\nu}{r} \right)^2} \right) \frac{E}{3}. \quad (21)$$

In what follows we shall refer to this equation as the “two-moment” closure.

3. Inner Boundary Condition

To construct the initial values for the moments at the neutrinosphere we adopt a steady state distribution f which is pure diagonal in the flavor basis at the neutrinosphere. The diagonal entries of the distribution matrix are of the form $f^{(aa)}(R_\nu, q, \theta) \propto Q_a(q) \Theta_a(\theta)$ with Q_a a function describing the energy spectrum for flavor a and

Θ_a a function describing the angular spectrum for flavor a . For simplicity, the energy spectra are taken to be Fermi Dirac distributions

$$Q_a(q) = \frac{1}{1 + \exp(q/(k_B T_a) - \eta_a)} \quad (22)$$

where T_a is the temperature and η_a is the chemical potential divided by $k_B T_a$. For both the moment-based and multi-angle calculations we adopt a uniform energy grid from 1 MeV to 60 MeV with 591 energy bins corresponding to an energy resolution of 100 keV. Repeating all calculations using a resolution of 50 keV indicates the numerical error is less than 0.1%. We adopt the parametric form for the initial angular distributions introduced by Mirizzi and Serpico [80]

$$\Theta_a(\theta) = \cos^{\beta_a} \theta. \quad (23)$$

The case of half isotropic emission corresponds to $\beta_a = 0$. Using these distributions we write

$$f^{(aa)}(R_\nu, q, \theta) = A_a (\beta_a + 2) Q_a(q) \Theta_a(\theta) \quad (24)$$

and imposing the requirement that the luminosity matrix L be given by equation (6) at the neutrinosphere R_ν , we find the constant A_a to be

$$A_a = \frac{\pi}{G_2(\eta)} \left(\frac{c}{R_\nu} \right)^2 \left(\frac{\hbar}{k_B T_a} \right)^3 \frac{L^{(aa)}}{\langle q \rangle_\nu}. \quad (25)$$

The function $G_2(\eta)$ is the complete Fermi-Dirac integral defined as

$$G_j(x) = \int_0^\infty \frac{t^j}{1 + \exp(t - x)} dt$$

and the quantity $\langle q \rangle_a$ is the mean energy given by

$$\langle q \rangle_a = \frac{\int F^{(aa)}(R_\nu, q) dq}{\int F^{(aa)}(R_\nu, q)/q dq}. \quad (26)$$

With the distribution matrix now defined, the energy density and flux moments at radius r (assuming no oscillations) are computed to be

$$E(r, q) = \frac{R_\nu^2}{2r^2} \left(\frac{q}{2\pi\hbar c} \right)^3 \begin{pmatrix} A_e Q_e(q) {}_2F_1 \left(1, \frac{1}{2}, 2 + \frac{\beta_e}{2}, \frac{R_\nu^2}{r^2} \right) & 0 \\ 0 & A_x Q_x(q) {}_2F_1 \left(1, \frac{1}{2}, 2 + \frac{\beta_x}{2}, \frac{R_\nu^2}{r^2} \right) \end{pmatrix} \quad (27)$$

$$F_r(r, q) = \frac{R_\nu^2}{2r^2} \left(\frac{q}{2\pi\hbar c} \right)^3 \begin{pmatrix} A_e Q_e(q) & 0 \\ 0 & A_x Q_x(q) \end{pmatrix} \quad (28)$$

$$P_{rr}(r, q) = \frac{R_\nu^2}{2r^2} \left(\frac{q}{2\pi\hbar c} \right)^3 \begin{pmatrix} A_e Q_e(q) {}_2F_1 \left(1, -\frac{1}{2}, 2 + \frac{\beta_e}{2}, \frac{R_\nu^2}{r^2} \right) & 0 \\ 0 & A_x Q_x(q) {}_2F_1 \left(1, -\frac{1}{2}, 2 + \frac{\beta_x}{2}, \frac{R_\nu^2}{r^2} \right) \end{pmatrix} \quad (29)$$

where ${}_2F_1(a, b, c, z)$ is the ordinary hypergeometric function. Similar expressions give the initial conditions for the antineutrino moments.

B. Numerical Method

To solve the quantum moment evolution equations we have developed a new code that computes the steady-state solution based on an inner boundary condition, given a specified matter density and electron fraction throughout the computational domain. We omit the collision terms in the moment evolution equations in order to focus our attention upon the oscillation physics. The code solves the equations using an explicit midpoint (second order Runge-Kutta) integrator. The radial step is adaptive based on the three frequencies associated with

the various flavor mixing terms in the Hamiltonian:

$$\begin{aligned} \omega_V &= \frac{\Delta m_{12}^2 c^4}{2\hbar q} \\ \omega_M &= \sqrt{2} G_F n_e / \hbar \\ \omega_{SI} &= \sqrt{\|H_{SI}\|_F^2 - \frac{1}{2} [Tr(H_{SI})]^2} / \hbar \end{aligned} \quad (30)$$

and $\|H_{SI}\|_F^2$ is the Frobenius norm of the self-interaction Hamiltonian, and $Tr(H_{SI})$ its trace. In the absence of the collision terms, the quantities $\|F_r\|_F^2 - \frac{1}{2} [Tr(F_r)]^2$ and $\|\bar{F}_r\|_F^2 - \frac{1}{2} [Tr(\bar{F}_r)]^2$ are conserved, i.e. independent of the radius r , for every energy. Our code enforces the conservation of these quantities to an error tolerance set to 0.1% per step. If the fractional change in the size of these quantities exceeds this bound, the time increment is halved and the step repeated. In what follows we present

the results from several test problems of the code.

III. TESTING MOMENT-BASED METHODS

If moment-based approaches to flavor oscillations are to be a feasible alternative to calculations based on discrete ordinates or other more exact approaches, the results must agree well with analytic predictions if they exist and/or the results from less approximate numerical approaches.

A. Constant Electron Density

Our first test case is flavor mixing of neutrinos emitted from a hard sphere of radius R_ν in a background of constant electron density. The flavor evolution for a single neutrino is well known for this scenario. The probability $P_T(r, \theta)$ that a neutrino initially in a particular flavor transitions to a neutrino of the opposite flavor after traveling a distance λ is given by a sinusoid with fixed amplitude and wavelength. Specifically,

$$P_T(r, \theta) = \sin^2(2\theta_{\text{MSW}}) \sin^2\left(\frac{\omega_{\text{MSW}} \lambda}{\hbar c}\right). \quad (31)$$

In this equation the effective matter mixing angle θ_{MSW} and effective frequency ω_{MSW} , are

$$\begin{aligned} \sin^2(2\theta_{\text{MSW}}) &= \frac{\sin^2(2\theta_{12})}{\sin^2(2\theta_{12}) + C^2} \\ \omega_{\text{MSW}} &= \frac{\omega_V}{2} \sqrt{\sin^2(2\theta_{12}) + C^2}, \end{aligned} \quad (32)$$

where

$$C = \cos(2\theta_{12}) \mp \frac{\omega_M}{\omega_V}. \quad (33)$$

The negative sign is used for neutrinos and the positive sign for antineutrinos.

Using equation (31), one can compute the angular moments of an ensemble of neutrinos by integrating the single neutrino solution over the solid angle with the appropriate $\cos\theta$ weight and taking into account the different path lengths λ from the emission point to the radial point of interest. However one does not need to do this calculation to predict what one should observe in the solutions. Due to the differing path lengths, the neutrinos will not all have the same phase of the flavor oscillations (i.e., they will be not all be coherent). The incomplete coherence will inevitably smear the oscillations of the moments compared to the flavor oscillations of a single neutrino.

The amount of coherence between the neutrinos on different trajectories is a function of the distance from the source. When the spread in path lengths to a given point is much smaller than the wavelength of the oscillations, all the neutrinos are very close to being coherent, but

as one moves away from the source the spread in path lengths grows and the amount of coherence drops. Far a neutrinosphere of radius R_ν , the path length difference between neutrinos emitted radially and those emitted at a tangent to the neutrinosphere asymptotes to R_ν . Thus the amount of coherence should also asymptote to a level determined by the ratio of the oscillation wavelength to R_ν .

In order to test our code's ability to reproduce these predictions we solve the two moment evolution equations and separately perform a multi-angle calculation using SQA. The spatial grid extends to 40 km, we use artificial vacuum mixing parameters of $\Delta m_{12}^2 = 6.9 \times 10^{-4} \text{ eV}^2$ and $\theta_{12} = 0.28818$ and consider monoenergetic neutrinos with an energy of $q = 1 \text{ MeV}$. The elements of the energy density moments are set arbitrarily according to the hierarchy $E^{(ee)}(R_\nu) = 10 \bar{E}^{(ee)}(R_\nu) = 100 E^{(xx)}(R_\nu) = 100 \bar{E}^{(xx)}(R_\nu)$. The matter density is set to $\rho = 8 \times 10^3 \text{ g cm}^{-3}$ and the electron fraction is $Y_e = 0.5$ in order to put the 1 MeV neutrinos close to the MSW resonance.

Figure 2 shows the oscillation probabilities as a function of the radius r for two angular distribution parameters of $\beta = 0$ (dashed red) and $\beta = 3$ (dashed purple). The electron neutrino and antineutrino transition probabilities are defined from the flux moment to be

$$P_{\nu_e \rightarrow \nu_x}(r) = \frac{r^2 F_r^{(xx)}(r) - R_\nu^2 F_r^{(xx)}(R_\nu)}{R_\nu^2 [F_r^{(ee)}(R_\nu) - F_r^{(xx)}(R_\nu)]} \quad (34)$$

$$P_{\bar{\nu}_e \rightarrow \bar{\nu}_x}(r) = \frac{r^2 \bar{F}_r^{(ee)}(r) - R_\nu^2 \bar{F}_r^{(xx)}(R_\nu)}{R_\nu^2 [\bar{F}_r^{(ee)}(R_\nu) - \bar{F}_r^{(xx)}(R_\nu)]}. \quad (35)$$

The top panel shows the flavor evolution as a function of radius for the neutrinos and the bottom panel for the antineutrinos. Although the neutrinos are on resonance and undergo nearly complete flavor oscillations, antineutrinos are off-resonance and only undergo minor flavor transformation. A comparison of the SQA results for the half-isotropic case and a separate, analytic integration of the survival probability, i.e.,

$$P_{\nu_e \rightarrow \nu_x}(r) = \frac{2r^2}{R_\nu^2} \int_{\cos\theta_{\text{max}}}^1 P_T(r, \theta) \cos\theta d(\cos\theta), \quad (36)$$

are visually indistinguishable.

The SQA results (dashed) display the decoherence effect of the neutrinos that have traveled along different trajectories leading to the reduction in the amplitude of the oscillations with increasing radius. Close to the neutrinosphere, the amplitudes of the flavor oscillations predicted from the moment code (solid) are similar in magnitude to the $\beta = 0$ SQA results (dashed purple). However, as the neutrinos move away, the moment code maintains larger flavor oscillations than exhibited in the multi-angle results.

Although the moment code overestimates the coherence of the neutrinos traveling along different trajectories, it does capture some phase effects. As the distribution becomes more forward-peaked, the average phase

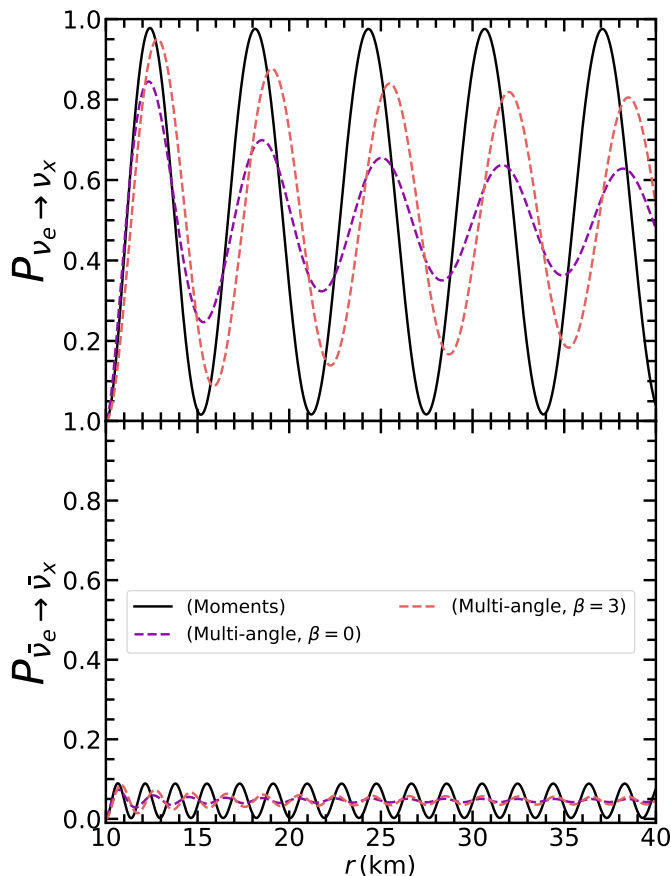


FIG. 2. Flavor oscillation test including vacuum and matter contributions to the Hamiltonian. Here we use $\Delta m_{12}^2 = 6.9 \times 10^{-4} \text{ eV}^2$ and $\theta_{12} = 0.28818$ in a background density profile of $\rho = 8000 \text{ g/cm}^3$ and $Y_e = 0.5$. The top panel shows the transition probability of electron neutrinos to x -flavor neutrinos while the bottom is the same for the antineutrinos. Solid lines are the results from the moment code and dashed lines are the results from the SQA using 90,001 angular bins.

advances more slowly due to smaller average path length to a given radial point. This can be seen by comparing the SQA results for $\beta = 3$ (forward-peaked) and $\beta = 0$ (semi-isotropic). The moment results, which have initial conditions corresponding to $\beta = 0$, show a more slowly evolving phase than the $\beta = 3$ results, just as the SQA $\beta = 0$ results do. However, the agreement does not last for long and a significant phase difference between the the moment and $\beta = 0$ oscillations exists at larger radius. Of course, in the limit of a perfectly forward-peaked distribution (not shown), the moment equations become increasingly accurate and agree increasingly well with multi-angle data.

| | L [ergs/s] | $\langle q \rangle$ [MeV] | T [MeV] | η | β | F_r/E | P_{rr}/E |
|---------------|-----------------------|---------------------------|-----------|--------|---------|---------|------------|
| ν_e | 4.1×10^{52} | 9.4 | 2.1 | 3.9 | 0.0 | 0.9975 | 0.995 |
| $\bar{\nu}_e$ | 4.3×10^{52} | 13.0 | 3.5 | 2.3 | 0.0 | 0.9975 | 0.995 |
| ν_x | 3.95×10^{51} | 15.8 | 4.4 | 2.1 | 0.0 | 0.9975 | 0.995 |
| $\bar{\nu}_x$ | 3.95×10^{51} | 15.8 | 4.4 | 2.1 | 0.0 | 0.9975 | 0.995 |

TABLE I. Parameters for the realistic collective oscillation simulation in Section III B 1. Listed are the neutrino luminosity L , average energy $\langle q \rangle$, temperature T , and chemical potential divided by the temperature η used in Equation 22. These are modified from the case of $p = 10$ and $q = 3.5$ (different from the q in this work that represents neutrino energy) from Table 6 in Keil *et al.* [81], with the electron flavor luminosities increased by a factor of 10. All angular distributions are described by $\beta = 0$ in Equation 23. The initial flux factors F_r/E and initial Eddington factors P_{rr}/E are also provided.

B. The Steady State Self Interaction Problem In Spherical Symmetry

Our final two tests are for the case of collective neutrino oscillations in an inhomogeneous environment. Collective flavor mixing is of interest for the study of core-collapse supernovae, as it is thought that such oscillations may occur at late times above the protoneutron star once the explosion has occurred. This may have a dramatic impact on the observed neutrino signal and nucleosynthesis in the CCSN environment [26]. Collective oscillations are well-studied in the steady state, free streaming approximation [82]. One of the distinct features of collective flavor mixing are the spectral swaps and splits that arise in the neutrino and antineutrino distributions at large radii (e.g., [83, 84]). This feature causes the neutrino spectra to deviate from the thermal-like spectra emitted from the neutrinosphere. It is also well established from such studies that the outcome of these calculations is heavily dependent on fully resolving the angular distribution of neutrinos [58]. This makes it a challenging test of a moment-based approach.

We present two simulations of this system using both the one-moment and two-moment closures in the following subsections. The first calculation in Section III B 1 is a reasonably realistic representation of the conditions outside a protoneutron star after the onset of explosion. The second calculation in Section III B 2 is a modified version of this setup, where we artificially adjust the parameters in order to probe the behavior of the moment method when flavor transformations occur in regions where the neutrino distribution is not highly forward-peaked.

1. Instability far from the neutrinosphere

In Table I we present the values for the neutrino luminosity L_ν , average energy $\langle q \rangle_\nu$, temperature T_ν , and chemical potential η_ν to be used in the first collective test calculation. These values are a modified version of

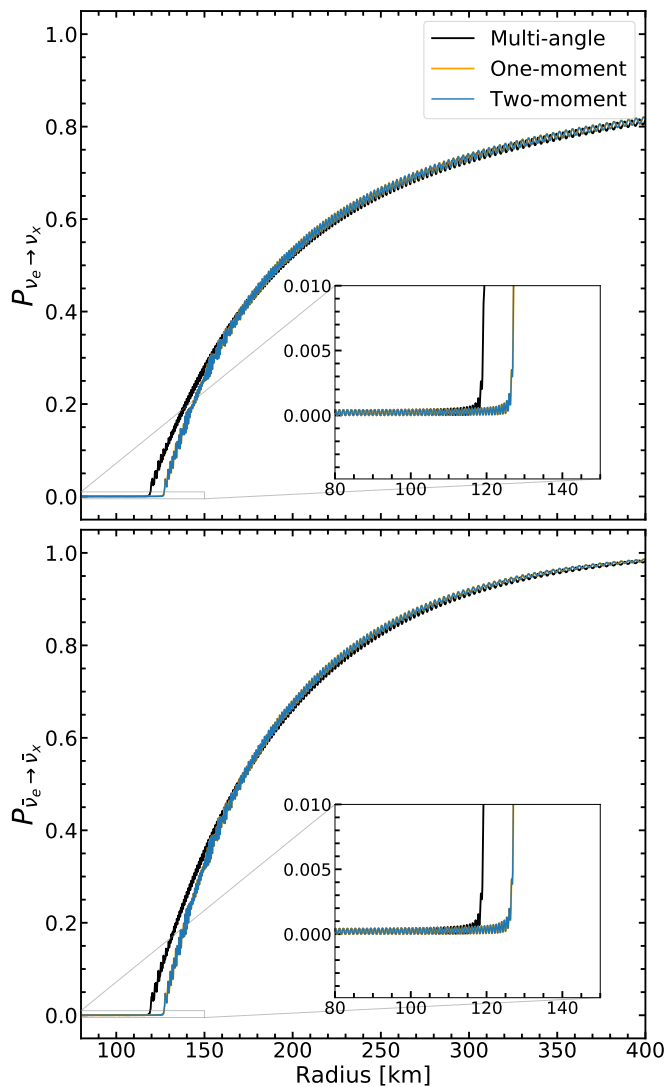


FIG. 3. The energy-integrated transition probability versus radius for the test in Section III B 1 and Table I. The top panel is for neutrinos and the bottom panel is for antineutrinos. The one-moment results are difficult to discern due to being largely obscured by the two-moment results.

the case $p = 10$ and $q = 3.5$ in Table 6 of Keil *et al.* [81], with the electron neutrino and antineutrino luminosities increased by a factor of 10. This makes the electron neutrino and electron antineutrino luminosities typical of what one expects during the accretion phase of an iron-core collapse supernova - see, for example, figure 2 in [85]. The inner computational boundary was chosen to be 100 km and the system was allowed to evolve until the neutrinos reached the radius of 400 km. We set the mixing parameters to $\Delta m_{12}^2 = -2.7 \times 10^{-3} \text{ eV}^2$ and $\theta_{12} = 0.01$. The neutrinosphere is set to $R_\nu = 10 \text{ km}$ for all neutrino and antineutrino flavors.

In Figure 3 we show the results of the calculation. The figure shows the energy-averaged transition probabilities defined using the radial component of the energy total,

| | L [ergs/s] | $\langle q \rangle$ [MeV] | T [MeV] | η | β | F_r/E | P_{rr}/E |
|---------------|------------------------|---------------------------|-----------|--------|---------|---------|------------|
| ν_e | 2.050×10^{49} | 9.4 | 2.1 | 3.9 | 0.0 | 0.5 | 0.33 |
| $\bar{\nu}_e$ | 2.550×10^{49} | 13.0 | 3.5 | 2.3 | 0.0 | 0.5 | 0.33 |
| ν_x | 1.698×10^{49} | 15.8 | 4.4 | 2.1 | 0.0 | 0.5 | 0.33 |
| $\bar{\nu}_x$ | 1.698×10^{49} | 15.8 | 4.4 | 2.1 | 0.0 | 0.5 | 0.33 |

TABLE II. Parameters for the collective oscillation simulation discussed in Section III B 2 designed to expose independent evolution of multiple moments. Listed are the luminosity L , average energy $\langle q \rangle$, temperature T , chemical potential divided by the temperature η , the angular distribution parameter β , the initial flux factor F_r/E and initial Eddington factor and P_{rr}/E at the neutrinosphere ($R_\nu = 10 \text{ km}$). Due to the rapid increase of the run time of the multi-angle calculation as the inner boundary is moved towards the neutrinosphere, the multi-angle calculation was started at 1 km above the neutrinosphere.

integrated fluxes $\vec{\mathcal{F}}_r$ to be

$$P_{\nu_e \rightarrow \nu_x}(r) = \frac{r^2 \mathcal{F}_r^{(xx)}(r) - R_\nu^2 \mathcal{F}_r^{(xx)}(R_\nu)}{R_\nu^2 [\mathcal{F}_r^{(ee)}(R_\nu) - \mathcal{F}_r^{(xx)}(R_\nu)]} \quad (37)$$

$$P_{\bar{\nu}_e \rightarrow \bar{\nu}_x}(r) = \frac{r^2 \bar{\mathcal{F}}_r^{(xx)}(r) - R_\nu^2 \bar{\mathcal{F}}_r^{(xx)}(R_\nu)}{R_\nu^2 [\bar{\mathcal{F}}_r^{(ee)}(R_\nu) - \bar{\mathcal{F}}_r^{(xx)}(R_\nu)]}. \quad (38)$$

In the figure we see the moment calculations exhibit a flavor instability at 126 km, similar to, but slightly larger than the radius of 119 km at which the flavor instability is seen in the multi-angle simulation. For both approaches, once the instability has begun we see that antineutrinos experience an almost complete flavor swap. The figure also indicates that there is little difference between the moment calculations that use the one-moment and two-moment closures. This similarity was not enforced nor expected and motivated the next test problem in Section III B 2.

There is also remarkable agreement between the flavor-transformed spectra between the moment and multi-angle methods. Figure 4 shows the initial and final spectra from the one-moment, two moment, and multi-angle calculations. In both the moment-based and multi-angle calculations, the antineutrino spectra show an almost complete swap between the $\bar{\nu}_e$ and $\bar{\nu}_x$ flavors and the neutrinos show a split in the spectra at about 25 MeV. This phenomenon has been seen many times in previous studies starting with Duan *et al.* [86, 87].

2. An instability close to the neutrinosphere

As we pointed out in Section III B 1, the high degree of concordance between the results using the one and two-moment closures was not enforced nor expected, but in hindsight is perhaps not surprising. At radii well beyond the neutrinosphere, there is very little difference between the flux and pressure moments, since the flux and Eddington factors are close to unity. One cannot expect to

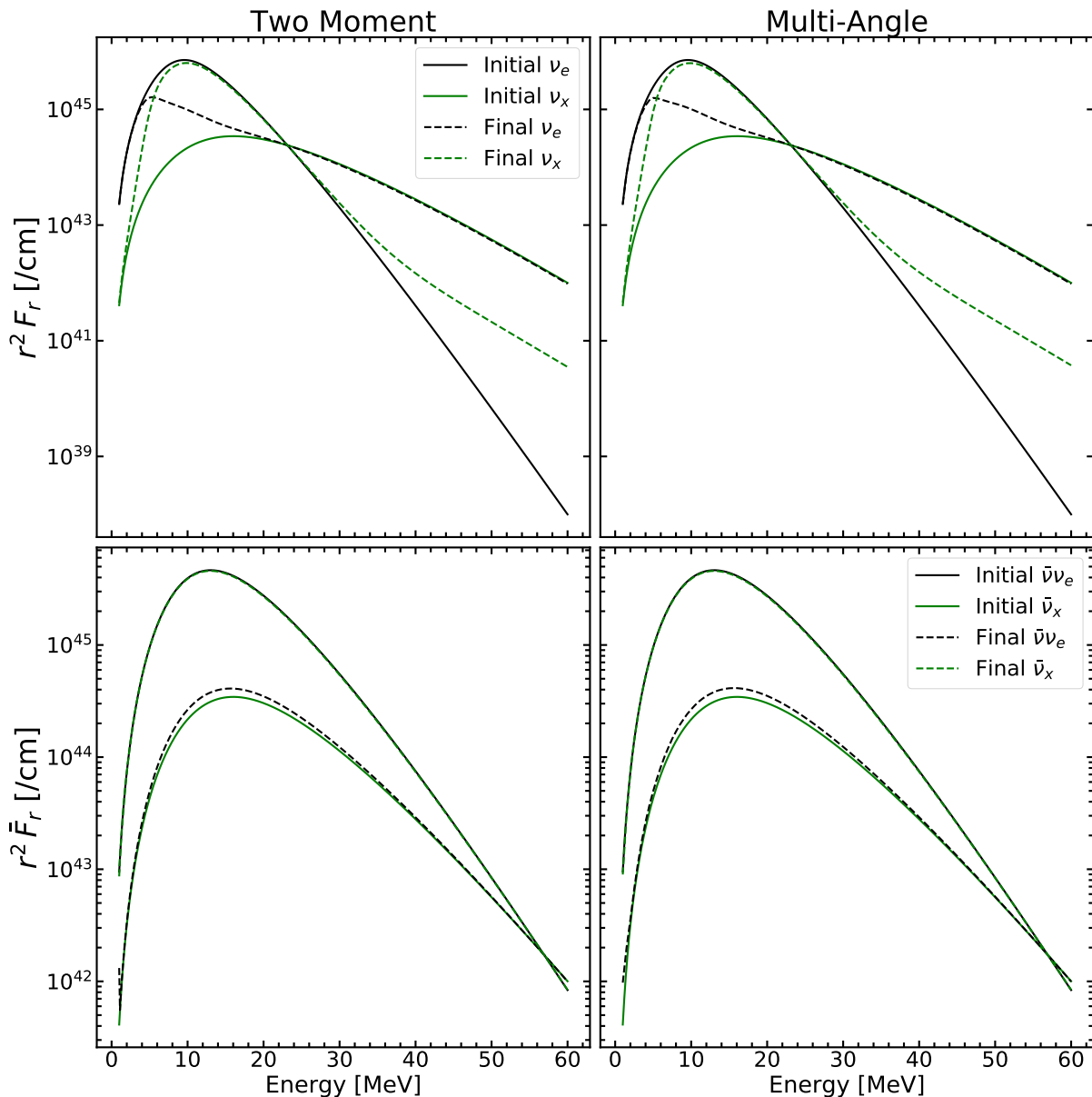


FIG. 4. Initial and final spectra versus energy for the test in Section III B 1 and Table I. Neutrinos are in the top two panels and antineutrinos are in the bottom two. The left column shows the two-moment simulation and the right column shows the multi-angle simulation. The black curves are the electron flavor and the green curves are the x flavor. The solid curves show the initial spectra and the dashed curves show the final spectra. The neutrino spectrum in all cases shows the spectral splits common in collective mixing. The antineutrinos show an almost complete spectral swap.

resolve fine angular features in a pencil-beam distribution using only coarse moments. If this interpretation is correct, we might reasonably expect to observe more significant differences between the one and two-moment calculations when flavor instabilities occur closer to the neutrinosphere (i.e., where the flux and Eddington factors are not close to unity). For this reason we present results from a second self-interaction test case where we engender flavor transformation closer to the neutrinosphere by artificially adjusting the neutrino luminosities. The new set of parameters we use for this calculation are shown

in Table II. In addition, for this test the inner boundary of the computational domain is at the neutrinosphere ($R_\nu = 10$ km).

The evolution of the energy-averaged transition probabilities from this second self-interaction calculation are shown in Figure 5. The system behaves similarly to the previous test problem studied in Section III B 1 in that the moment calculations (blue and orange) closely track each other and exhibit an onset of flavor transformation in approximately the same location as in the multi-angle calculations. However, due to the decreased neutrino

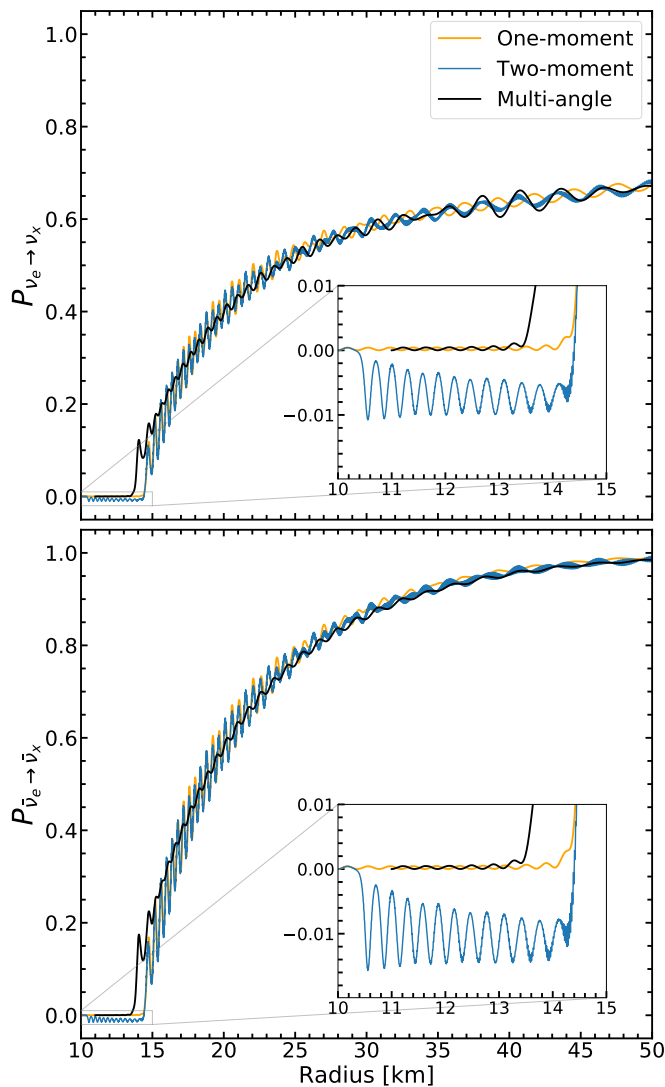


FIG. 5. Transition probability versus radius for energy-integrated neutrinos for the modified collective oscillation test in Section III B 2 and Table II. The top panel is for neutrinos and bottom panel is for antineutrinos. The orange curve shows the one-moment simulation, blue curve shows the two-moment simulation, and the green curve shows the multi-angle simulation.

luminosities, the instability starts at $r \approx 14$ km, much closer to the neutrinosphere than the onset at $r \approx 120$ km in Section III B 1. The moment calculations agree with the multi-angle calculations about the onset of the instability even better than in the previous case.

In the insets in Figure 5, we show the transition probabilities for during the first five kilometers of the calculation. We observe that the transition probability from the multi-angle and one-moment calculations are small and positive over this region, but that the two-moment calculation shows slightly negative probabilities until significant flavor conversion occurs at 14 km. Our investigation into the origin of the negative probabilities are

presented in Appendix B. The negative probabilities in the two-moment calculations are not a numerical error and are likely due to the closure.

The similarity between the results for the one- and two-moment closures shown in Figure 5 cannot be attributed to the fact that the flux and Eddington factors are close as in Section III B 1. Instead, we have found that this behavior arises because our choice of closure is so self-consistent that the evolution equation for the flux (Equation 8) is essentially identical using both the one-moment and two-moment closures. Thinking first about the analytic relationships for the moments in a bulb model without flavor transformation, one can relate the pressure to the flux as $P_{rr} = D(r) F_r$, where $D(r)$ is a scalar function given by

$$D(r) = \frac{2(1 + \cos \theta_{max} + \cos^2 \theta_{max})}{3(1 + \cos \theta_{max})}, \quad (39)$$

$$= \frac{2}{3r} \left(\frac{2r^2 - R_\nu^2 + r\sqrt{r^2 - R_\nu^2}}{r + \sqrt{r^2 - R_\nu^2}} \right).$$

Inserting this relationship into Equations 8 and 10, the evolution equation for the steady-state flux in the two-moment approach becomes the same as the radial evolution of the steady state flux using the one-moment closure, indicating the self-consistency of our choice of closures. Thus, wherever the flux and pressure as calculated by the two-moment approach are related by Equation 39, the evolution of the flux (and thus the transition probability) in the one- and two-moment systems will evolve identically.

To examine whether this coherence of the flux and pressure moment actually occurs in our calculations, in Figure 6 we plot $D(r)$ (orange) together with the ratio

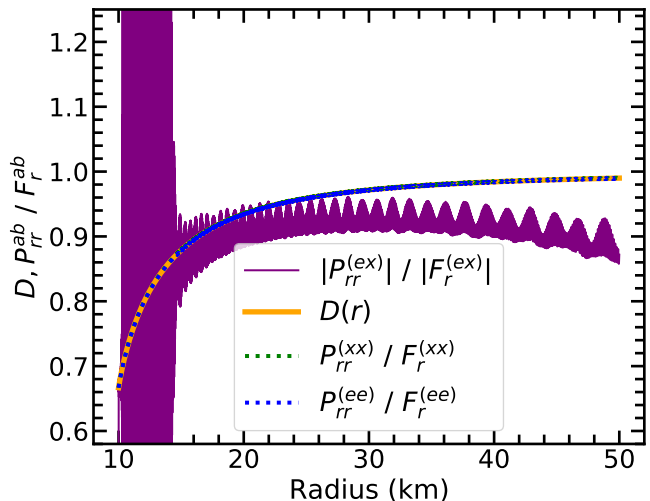


FIG. 6. The ratio of the elements from the pressure tensor to the corresponding elements from the flux as a function of the radius r for the 15 MeV neutrinos in the two-moment calculation using the parameters given in Section III B 2 and Table II.

of the corresponding elements from the pressure and flux moments for the 15 MeV neutrinos. We find the ratios of $P_{rr}^{(ee)}/F_r^{(ee)}$ (blue dashed) and $P_{rr}^{(xx)}/F_r^{(xx)}$ (green dashed, not visible under the blue dashed curve) match the function $D(r)$ very well, indicating that the diagonal moments grow and shrink due to flavor transformation at the same rate. The ratio $|P_{rr}^{(ex)}|/|F_r^{(ex)}|$ (purple) does not follow $D(r)$ before the instability, as the flavor off-diagonal elements are very small. Once flavor transformation begins at $r \sim 14$ km, the flavor off-diagonal ratio more closely follows $D(r)$, though not as well as the diagonal elements.

Figure 7 shows the phase angle difference $\xi = \arg(P_{rr}^{(ex)}) - \arg(F_r^{(ex)})$ between the off-diagonal elements of the flux and pressure moments from the two-moment and multi-angle calculations. The figure shows how the phase difference for the multi-angle calculation is always small, indicating that the flux and pressure moments experience tightly coupled evolution. The phase difference in the two-moment calculation is initially highly variable, since the off-diagonal components are very small. However, once the flavor transformation begins around $r = 14$ km, the two moments become very coherent and the phase difference does not exceed a few degrees. Taken together, Figures 6 and 7 show that $P_{rr} = D(r)F_r$ is a good approximation for this problem and the coherence between the two moments reduces the system of moment equations to that for a single moment. Note that this coherence between the pressure and flux in the two-moment scheme is not imposed; it emerges as the calculation proceeds.

Finally, Figure 8 shows the spectra of the neutrinos and antineutrinos at 50 km from the two-moment and multi-angle calculations. The spectra from the two methods

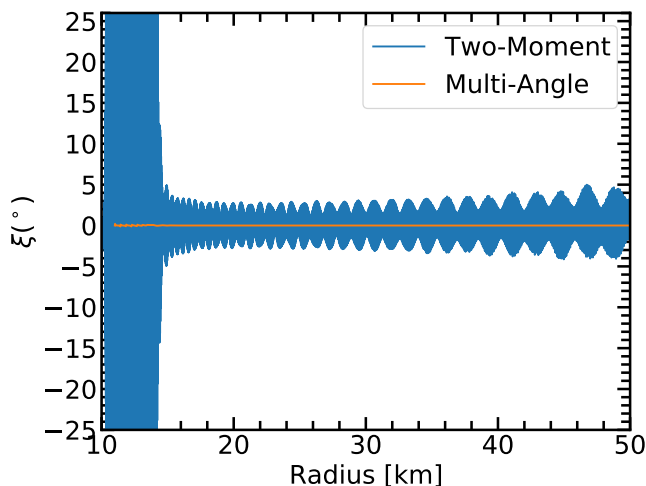


FIG. 7. The difference between the phase angles of the off-diagonal elements of the pressure and flux moments for 15 MeV neutrinos from the two-moment simulation (cyan) and the multi-angle simulation (orange) in the modified collective oscillation setup of Section III B 2 and Table II.

agrees well with only slight differences in the high-energy tails. The moment-based approach accurately calculates the spectral evolution as well as the gross, integrated behavior.

IV. DISCUSSION & CONCLUSIONS

We have presented here a method for modeling neutrino flavor mixing using one and two moments. We then investigated how well it captures the mixing effects of analytic predictions and of more exact but more computationally expensive multi-angle calculations by considering three problems in a bulb-model geometry representative of core-collapse supernovae.

The first problem was the flavor evolution of neutrinos emitted from a neutrino bulb in matter with a density chosen to put the 1 MeV neutrinos on the MSW resonance for the given mixing parameters. We found that the moment calculations overestimated the amplitude of the flavor mixing at a given radial point because they were not able to accurately account for the incoherence of neutrinos which had traveled along different trajectories. As the emission at the neutrinosphere becomes more forward-peaked i.e. a greater proportion of the neutrinos are emitted along trajectories close to the radial direction, the transition probabilities from the multi-angle calculation become more similar with those from the moment calculation.

The last two test problems were used to study the case of collective flavor transformation due to neutrino self interaction. In the first of these calculations, designed with a reasonably realistic inner boundary condition, the moment and multi-angle results were in good agreement in that the onset of the transformation differed by just a few kilometers. The results from the one-moment and two-moment calculations were almost identical. When we adjusted the parameters so as to produce flavor transformation much closer to the neutrinosphere (i.e., where the flux and Eddington factors are much lower), we again found the multi-angle and moment calculations were in good agreement on where the flavor transformation begins and that, once again, the one-moment and two-moment calculations yield essentially the same radial evolution of the transition probability. We then demonstrated that the similarity of the two moment-based approaches is due to a sustained synchronization between the flux and pressure moments which effectively collapses the tower of moment equations to that for a single moment. This coherence between the flux and pressure moments appears to emerge naturally in steady state self-interaction situations.

Overall, the various tests we undertook indicate that moment-based approach does well at capturing the overall neutrino flavor transformation seen in the more computationally expensive, multi-angle, calculation. The onset of flavor mixing is predicted with an accuracy of a few kilometers and the spectra are similar. However we

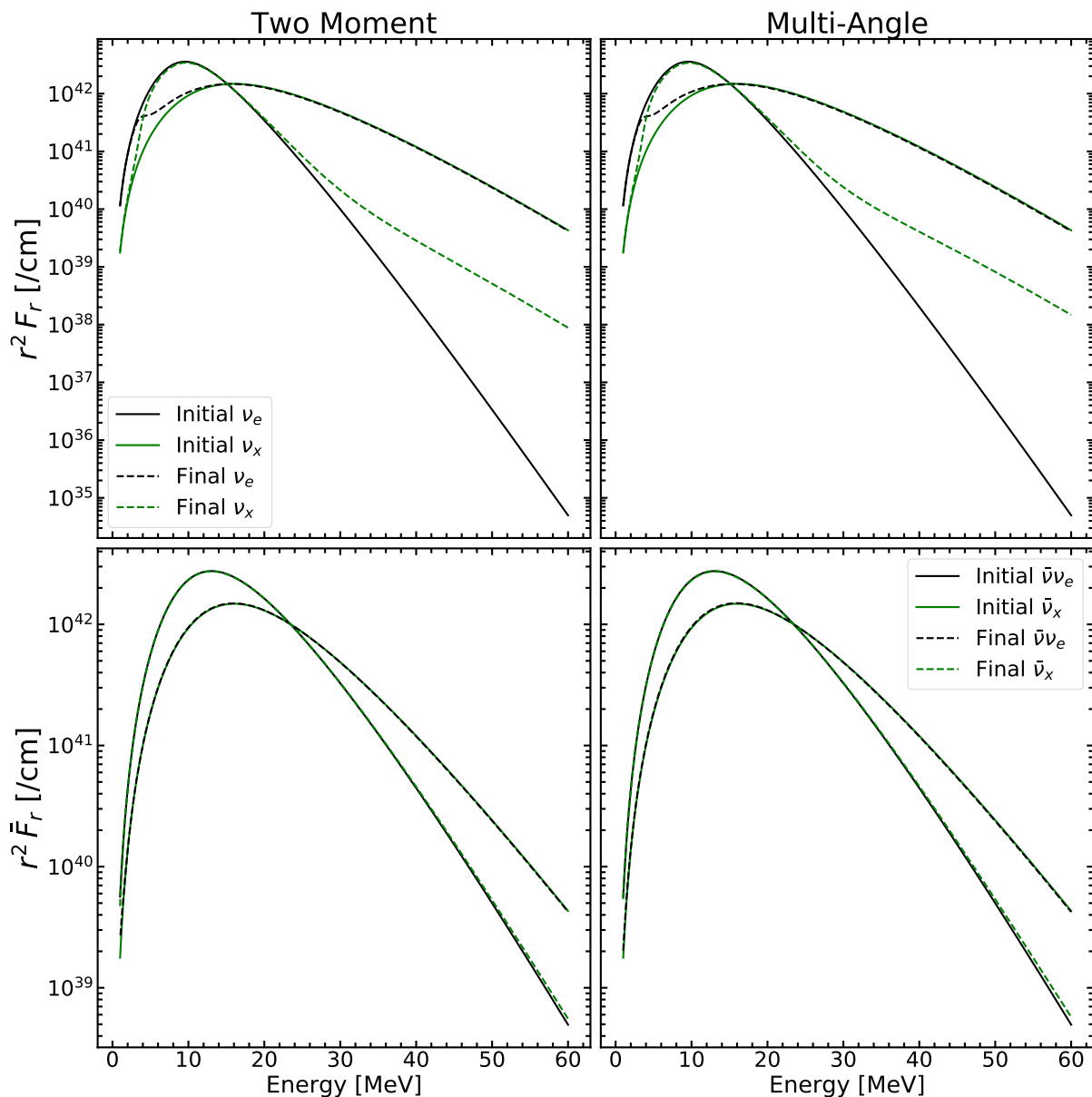


FIG. 8. Initial and final spectra versus energy for neutrinos from simulations using parameters in Table II and Section III B 2. Neutrinos are in the top two panels and antineutrinos are in the bottom two. The left column shows the two-moment simulation and the right column shows the multi-angle simulation. The black lines are the electron flavor and the green lines are the x flavor. The solid lines show the initial spectra and the dashed lines show the final spectra.

do find differences between the two approaches and our final test problem also revealed that the moment-based approaches can yield, at least temporarily, unphysical solutions. One may speculate that the differences are due to the closure. The closures we have used in this paper are scalar relations but in general, for quantum moments, one would expect phase differences between the off-diagonal elements of the two moments used in the closure which a scalar closure cannot generate. To permit the phase differences to appear one requires a more general, quantum closure. We shall explore quantum closures in future work.

In summary, our results indicate that moment-based schemes are an inexpensive approach to neutrino transport that are able to capture most of the flavor mixing phenomenology seen in more-exact, but more expensive, calculations. We caution that any enthusiasm for a moment-based approach to neutrino oscillations must be tempered by remembering that any approach which truncates the tower of moment equations cannot converge to those from the full quantum kinetic equations and thus moment-based approaches will continue to require verification against those derived from less approximate methods. Should further, more demanding com-

parisons of moments and less approximate methods, (especially comparisons which do not assume steady state) reveal that moment-based methods perform well in those situations too, we would proffer moment methods are a promising and viable avenue for including neutrino transformation in hydrodynamical simulations.

ACKNOWLEDGMENTS

The authors would like to thank S. Couch and E. P. O’Connor for their advice and support through this project. MLW was supported by a NSF Astronomy and Astrophysics Postdoctoral Fellowship under award AST-1801844. TC, MM, JPK, GCM, EG, and CF are supported by the DOE Office of Nuclear Physics award DE-FG02-02ER41216. E. G. acknowledges support by the National Science Foundation grant No. PHY-1430152 (JINA Center for the Evolution of the Elements). This work was partially enabled by the National Science Foundation under grants No. PHY-1630782 (N3AS hub) and No. PHY-2020275 (N3AS PFC). SR was supported by a NSF Astronomy and Astrophysics Postdoctoral Fellowship under award AST-2001760. The calculations presented in this paper were undertaken with the support of Michigan State University through computational resources provided by the Institute for Cyber-Enabled Research, and on the *Payne* machine at NCSU which is supported in part by the Research Corporation for Science Advancement. The authors would like to acknowledge the use of the following software: Matplotlib [88], Numpy [89], and SciPy [90].

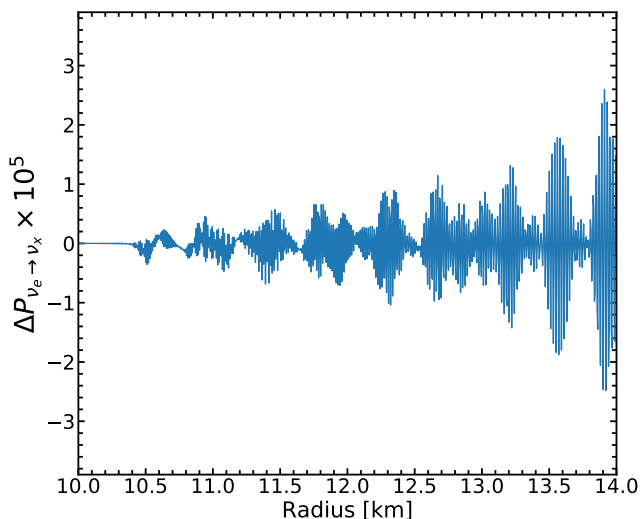


FIG. 9. The difference in the transition probability as a function of radius for the 15 MeV neutrinos from a two-moment calculation with an energy resolution of 50 keV compared to the fiducial energy resolution of 100 keV. The calculation uses the parameters shown in Table II.

Appendix A: SQA

For the multi-angle calculations we use SQA, which is an implementation of the Bulb Model described in Duan *et al.* [91]. The momenta of the neutrinos and antineutrinos at the neutrinosphere are discretized into N_E energy bins and N_A angle bins. The energy resolution is uniform, but for the direction we adopt uniform resolution in the quantity $u = \sin^2 \theta_R$ where θ_R is the angle at which the neutrino was emitted at the neutrinosphere relative to the radial direction. This distribution gives greater weight to the angles emitted at large angles θ_R , since these rays have the largest dispersion in path lengths from the neutrinosphere to a given radial point. We introduce an evolution matrix S that relates the initial density matrix for neutrinos moving with each momentum \vec{p}_0 at the neutrinosphere to the density matrix for neutrinos moving at some distance λ along the same trajectory with momentum $\vec{p}(\lambda)$. That is,

$$\rho(\lambda, \vec{p}_0) = S(\lambda, \vec{p}_0) \rho(R_\nu, \vec{p}_0) S^\dagger(\lambda, \vec{p}_0). \quad (\text{A1})$$

A matrix $\bar{S}(\lambda, \vec{p}_0)$ plays the same role for antineutrinos. The matrix $S(\lambda, \vec{p}_0)$ evolves according to the Schrödinger equation

$$i \frac{dS}{d\lambda} = H(\lambda, \vec{p}) S. \quad (\text{A2})$$

For the antineutrinos, the matrix \bar{S} similarly evolves according to the Hamiltonian \bar{H} . As in the moment method described in Section II, the Hamiltonian is composed of three parts: vacuum H_V , matter H_M , and self-interaction H_{SI} . The vacuum and matter terms were given previously in Equations 14 and 15, and the self interaction term is

$$H_{\text{SI}}(r, \vec{p}) = \sqrt{2} G_F \int (1 - \hat{\mathbf{p}} \cdot \hat{\mathbf{q}}) [\rho(r, \vec{q}) - \bar{\rho}^*(r, \vec{q})] q^2 dq d\Omega. \quad (\text{A3})$$

The density matrices are evolved to discrete radial points $r(\lambda)$ common among all trajectories so the Hamiltonian can be straightforwardly integrated.

To ensure unitarity, the matrices S and \bar{S} are parameterized by four real variables: three are the angles defining a unit vector in a four-dimensional Euclidian flavor space, and the fourth is the phase of the determinant. The differential equations for all of the parameters are solved simultaneously with an explicit Runge-Kutta integrator that uses an adaptive step size and the Cash-Karp parameter set. Several sources of numerical errors in multi-angle codes have been identified over the years [57, 58, 92, 93]. The numerical accuracy of the SQA calculations presented in this paper is estimated to be less than 1% based on the lack of visible differences between the results using different numbers of energy or angle bins, and initial radii. A related code, Isotropic-SQA, was used for solving the neutrino quantum kinetic equations in isotropic and homogeneous conditions [94] is available at [71].

Appendix B: Numerical Errors in the Moment-Based Calculations

During our examination of the results from the moment-based code using the two-moment closure, we observed that the transition probability became slightly and temporarily negative, as shown in the inset of Figure 5. The transition probabilities from the code using the one-moment closure scheme did not contain this feature. We have explored the reason for the appearance of negative probabilities in the results from the two-moment scheme and attempted several strategies to remove them. In this appendix we describe those efforts.

The negative probabilities are present only when the self-interaction contribution to the Hamiltonian is included, and they occur for both neutrinos and antineutrinos. We do not believe the negative probabilities to be due to a numerical errors from the ODE integrator, since decreasing the error tolerance for the integrator does not improve the solution. We also changed the algorithm from an explicit second-order ‘midpoint’ Runge-Kutta integrator to an adaptive step size routine using the Cash-Karp parameter set and a fractional error tolerance per step of 10^{-10} , and found the negative probabilities persisted. We then changed the parameterization of the moment matrices by writing the diagonal elements as $M^{(ee)} = Tr(M) \cos^2 \theta_M$ and $M^{(xx)} = Tr(M) \sin^2 \theta_M$ where $Tr(M)$ is the trace and θ_M an angle, in an effort to prohibit the unphysical behavior of the diagonal elements. However, when we ran our code using the two-moment closure to evolve these new parameters, the code terminated prematurely when the step size shrank to zero at the point where the original version crossed into the unphysical solution space.

The negative probabilities are not dependent upon the number of energy bins used in the calculation. While the results in Section III B 2 use an energy resolution of 100 keV, we repeated the calculation using an energy resolution of 50 keV. The evolution of the transition probability for the 15 MeV neutrinos from the two calculations is shown in Figure 9. We observe changes in the transition probability that are of order 0.001% in the interval $10 \text{ km} \leq r \leq 14 \text{ km}$ where the negative probabilities appear. We also ran a single energy calculation for which energy resolution is not a factor using an energy of 5 MeV. The choice of 5 MeV produces an onset of flavor transformation at $r \approx 13.5 \text{ km}$, similar to that seen in the multi-energy calculation. The results from this

single-energy calculation shown in Figure (10) produce similar negative transition probabilities. Thus we do not believe numerical error from the energy resolution to be the origin of the negative probabilities.

Note that the first term on the right hand side of the moment evolution equations (Equations 8-11) unitarily evolves the moment’s flavor structure and cannot lead to negative probabilities except for numerical error. The geometrical term (the last term on the left hand side of the equation) also leads to non-unitary evolution, but the

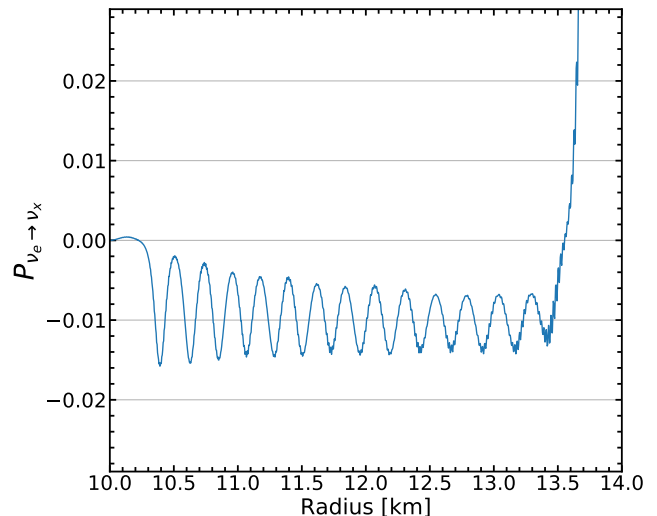


FIG. 10. The transition probability as a function of radius as computed from a single-energy calculation using the parameters shown in Table II. The energy of the neutrinos and antineutrino is chosen to be 5 MeV in order to produce an instability in approximately the same location seen in the multi-energy calculation.

form of the equations implemented in the code evolves a variable constructed by multiplying moments by r^2 such that this geometrical term disappears and also cannot lead to the problems we see. The second commutator on the right hand side is a final source of physical non-unitary evolution of the moments and depends on the choice of closure and energy integrals of the moments. Since we do not believe the energy integrals to be the source of the error, we are inclined to believe that the closure we use, while geometrically justified and always realizable, may not be sufficient to enforce physical evolution of the moment equations. However, an analysis of various options for closures is beyond the scope of this paper.

-
- [1] S. A. Colgate and R. H. White, The Hydrodynamic Behavior of Supernovae Explosions, *The Astrophysical Journal* **143**, 626 (1966).
 [2] H. A. Bethe, Supernova mechanisms, *Reviews of Modern Physics* **62**, 801 (1990), publisher: American Physical

Society.

- [3] K. Kotake, K. Sato, and K. Takahashi, Explosion mechanism, neutrino burst and gravitational wave in core-collapse supernovae, *Reports on Progress in Physics* **69**, 971 (2006).

- [4] H. T. Janka, K. Langanke, A. Marek, G. Martínez-Pinedo, and B. Müller, Theory of core-collapse supernovae, *Physics Reports The Hans Bethe Centennial Volume 1906-2006*, **442**, 38 (2007).
- [5] H.-T. Janka, Explosion Mechanisms of Core-Collapse Supernovae, *Annual Review of Nuclear and Particle Science* **62**, 407 (2012).
- [6] A. Burrows, Colloquium: Perspectives on core-collapse supernova theory, *Reviews of Modern Physics* **85**, 245 (2013), publisher: American Physical Society.
- [7] T. Foglizzo, R. Kazeroni, J. Guilet, F. Masset, M. González, B. K. Krueger, J. Novak, M. Oertel, J. Margueron, J. Faure, N. Martin, P. Blottiau, B. Peres, and G. Durand, The Explosion Mechanism of Core-Collapse Supernovae: Progress in Supernova Theory and Experiments, *Publications of the Astronomical Society of Australia* **32**, 10.1017/pasa.2015.9 (2015), publisher: Cambridge University Press.
- [8] E. J. Lentz, S. W. Bruenn, W. R. Hix, A. Mezzacappa, O. E. B. Messer, E. Endeve, J. M. Blondin, J. A. Harris, P. Marronetti, and K. N. Yakunin, THREE-DIMENSIONAL CORE-COLLAPSE SUPERNOVA SIMULATED USING A 15 M \dot{M} PROGENITOR, *The Astrophysical Journal* **807**, L31 (2015).
- [9] B. Müller, T. Melson, A. Heger, and H.-T. Janka, Supernova simulations from a 3D progenitor model – Impact of perturbations and evolution of explosion properties, *Monthly Notices of the Royal Astronomical Society* **472**, 491 (2017).
- [10] C. D. Ott, L. F. Roberts, A. d. S. Schneider, J. M. Fedrow, R. Haas, and E. Schnetter, The Progenitor Dependence of Core-collapse Supernovae from Three-dimensional Simulations with Progenitor Models of 12–40 M \dot{M} , *The Astrophysical Journal* **855**, L3 (2018).
- [11] A. Summa, H.-T. Janka, T. Melson, and A. Marek, Rotation-supported Neutrino-driven Supernova Explosions in Three Dimensions and the Critical Luminosity Condition, *The Astrophysical Journal* **852**, 28 (2018), publisher: American Astronomical Society.
- [12] E. P. O’Connor and S. M. Couch, Exploring Fundamentally Three-dimensional Phenomena in High-fidelity Simulations of Core-collapse Supernovae, *The Astrophysical Journal* **865**, 81 (2018).
- [13] K. Nakamura, T. Takiwaki, and K. Kotake, Long-term simulations of multi-dimensional core-collapse supernovae: Implications for neutron star kicks, *Publications of the Astronomical Society of Japan* **71**, 10.1093/pasj/psz080 (2019).
- [14] R. Glas, H. T. Janka, T. Melson, G. Stockinger, and O. Just, Effects of LESA in Three-dimensional Supernova Simulations with Multidimensional and Ray-by-ray-plus Neutrino Transport, *The Astrophysical Journal* **881**, 36 (2019).
- [15] R. Glas, Three-dimensional Core-collapse Supernova Simulations with Multidimensional Neutrino Transport Compared to the Ray-by-ray-plus Approximation, *The Astrophysical Journal* **873**, 10.3847/1538-4357/ab0423 (2019).
- [16] A. Burrows, D. Radice, D. Vartanyan, H. Nagakura, M. A. Skinner, and J. C. Dolence, The overarching framework of core-collapse supernova explosions as revealed by 3D fornaX simulations, *Monthly Notices of the Royal Astronomical Society* **491**, 2715 (2020).
- [17] H. Yasin, S. Schäfer, A. Arcones, and A. Schwenk, Equation of State Effects in Core-Collapse Supernovae, *Phys. Rev. Lett.* **124**, 092701 (2020).
- [18] A. da Silva Schneider, E. O’Connor, E. Granqvist, A. Betranhandy, and S. M. Couch, Equation of State and Progenitor Dependence of Stellar-mass Black Hole Formation, *The Astrophysical Journal* **894**, 4 (2020), arXiv:2001.10434 [astro-ph.HE].
- [19] S. Ghosh, N. Wolfe, and C. Fröhlich, PUSHING core-collapse supernovae to explosions in spherical symmetry V: Equation of state dependency of explosion properties, nucleosynthesis yields, and compact remnants, arXiv e-prints, arXiv:2107.13016 (2021), arXiv:2107.13016 [astro-ph.HE].
- [20] D. Radice, C. D. Ott, E. Abdikamalov, S. M. Couch, R. Haas, and E. Schnetter, Neutrino-driven convection in core-collapse supernovae: high-resolution simulations, *The Astrophysical Journal* **820**, 76 (2016).
- [21] S. Richers, H. Nagakura, C. D. Ott, J. Dolence, K. Sumiyoshi, and S. Yamada, A Detailed Comparison of Multidimensional Boltzmann Neutrino Transport Methods in Core-collapse Supernovae, *The Astrophysical Journal* **847**, 133 (2017).
- [22] E. O’Connor, R. Bollig, A. Burrows, S. Couch, T. Fischer, H.-T. Janka, K. Kotake, E. J. Lentz, M. Liebendörfer, O. E. B. Messer, A. Mezzacappa, T. Takiwaki, and D. Vartanyan, Global comparison of core-collapse supernova simulations in spherical symmetry, *Journal of Physics G Nuclear Physics* **45**, 104001 (2018).
- [23] O. Just, R. Bollig, H.-T. Janka, M. Obergaulinger, R. Glas, and S. Nagataki, Core-collapse supernova simulations in one and two dimensions: comparison of codes and approximations, *Monthly Notices of the Royal Astronomical Society* **481**, 4786 (2018).
- [24] B. Dasgupta, E. P. O’Connor, and C. D. Ott, Role of collective neutrino flavor oscillations in core-collapse supernova shock revival, *Physical Review D* **85**, 065008 (2012).
- [25] C. J. Stapleford, C. Fröhlich, and J. P. Kneller, Coupling neutrino oscillations and simulations of core-collapse supernovae, *Physical Review D* **102**, 081301 (2020).
- [26] H. Duan, G. M. Fuller, and Y.-Z. Qian, Collective Neutrino Oscillations, *Annual Review of Nuclear and Particle Science* **60**, 569 (2010).
- [27] G. Bellini, L. Ludhova, G. Ranucci, and F. L. Villante, Neutrino Oscillations, *Advances in High Energy Physics* **2014**, 1 (2014).
- [28] S. P. Mikheyev and A. Y. Smirnov, Resonance enhancement of oscillations in matter and solar neutrino spectroscopy, *Yad. Fiz.* **42**, 1441 (1985), (*Sov. J. Nucl. Phys.* **42** 913).
- [29] S. P. Mikheyev and A. Y. Smirnov, Neutrino oscillations in matter with varying density, in *’86 Massive Neutrinos in Astrophysics and in Particle Physics*, edited by O. Frackler and J. Trân Thanh Vân (Editions Frontières, Gif-sur-Yvette, 1986) p. 355.
- [30] L. Wolfenstein, Neutrino oscillations in matter, *Phys. Rev. D* **17**, 2369 (1978).
- [31] J. P. Kneller, G. C. McLaughlin, and J. Brockman, Oscillation Effects and Time Variation of the Supernova Neutrino Signal, *Phys. Rev. D* **77**, 045023 (2008),

- arXiv:0705.3835 [astro-ph].
- [32] J. Gava, J. Kneller, C. Volpe, and G. C. McLaughlin, A Dynamical collective calculation of supernova neutrino signals, *Phys. Rev. Lett.* **103**, 071101 (2009), arXiv:0902.0317 [hep-ph].
- [33] K. M. Patton, J. P. Kneller, and G. C. McLaughlin, Stimulated Neutrino Transformation Through Turbulence, *Phys. Rev. D* **89**, 073022 (2014), arXiv:1310.5643 [hep-ph].
- [34] S. Chakraborty, T. Fischer, A. Mirizzi, N. Saviano, and R. Tomas, No Collective Neutrino Flavor Conversions during the Supernova Accretion Phase, *Physical Review Letters* **107**, 151101 (2011), publisher: American Physical Society.
- [35] H. Duan and A. Friedland, Self-Induced Suppression of Collective Neutrino Oscillations in a Supernova, *Physical Review Letters* **106**, 091101 (2011).
- [36] C. J. Stappelford, D. J. Väänänen, J. P. Kneller, G. C. McLaughlin, and B. T. Shapiro, Nonstandard Neutrino Interactions in Supernovae, *Phys. Rev. D* **94**, 093007 (2016), arXiv:1605.04903 [hep-ph].
- [37] R. F. Sawyer, Speed-up of neutrino transformations in a supernova environment, *Physical Review D* **72**, 045003 (2005).
- [38] R. F. Sawyer, Neutrino cloud instabilities just above the neutrino sphere of a supernova, *Physical Review Letters* **116**, 081101 (2016).
- [39] S. Chakraborty, R. S. Hansen, I. Izaguirre, and G. Raffelt, Self-induced neutrino flavor conversion without flavor mixing, *Journal of Cosmology and Astroparticle Physics* **2016** (03), 042.
- [40] I. Izaguirre, G. Raffelt, and I. Tamborra, Fast Pairwise Conversion of Supernova Neutrinos: A Dispersion Relation Approach, *Physical Review Letters* **118**, 021101 (2017).
- [41] F. Capozzi, B. Dasgupta, E. Lisi, A. Marrone, and A. Mirizzi, Fast flavor conversions of supernova neutrinos: Classifying instabilities via dispersion relations, *Physical Review D* **96**, 043016 (2017).
- [42] B. Dasgupta and M. Sen, Fast neutrino flavor conversion as oscillations in a quartic potential, *Physical Review D* **97**, 023017 (2018).
- [43] S. Abbar and H. Duan, Fast neutrino flavor conversion: Roles of dense matter and spectrum crossing, *Physical Review D* **98**, 043014 (2018).
- [44] L. Johns, H. Nagakura, G. M. Fuller, and A. Burrows, Neutrino oscillations in supernovae: angular moments and fast instabilities, *Phys. Rev. D* **101**, 043009 (2020), arXiv:1910.05682 [hep-ph].
- [45] F. Capozzi, S. Abbar, R. Bollig, and H. T. Janka, Fast neutrino flavor conversions in one-dimensional core-collapse supernova models with and without muon creation, *Phys. Rev. D* **103**, 063013 (2021), arXiv:2012.08525 [astro-ph.HE].
- [46] L. Johns and H. Nagakura, Fast flavor instabilities and the search for neutrino angular crossings, *Phys. Rev. D* **103**, 123012 (2021), arXiv:2104.04106 [hep-ph].
- [47] H. Nagakura, L. Johns, A. Burrows, and G. M. Fuller, Where, when and why: occurrence of fast-pairwise collective neutrino oscillation in three-dimensional core-collapse supernova models, *Phys.Rev.D* **104**, 083025 (2021), arXiv:2108.07281 [astro-ph].
- [48] H. Nagakura and L. Johns, Constructing angular distributions of neutrinos in core-collapse supernovae from zeroth and first moments calibrated by full Boltzmann neutrino transport, *Phys. Rev. D* **103**, 123025 (2021), arXiv:2104.05729 [astro-ph.HE].
- [49] S. Abbar and M. C. Volpe, On fast neutrino flavor conversion modes in the nonlinear regime, *Physics Letters B* **790**, 545 (2019).
- [50] S. Shalgar and I. Tamborra, On the Occurrence of Crossings between the Angular Distributions of Electron Neutrinos and Antineutrinos in the Supernova Core, *The Astrophysical Journal* **883**, 80 (2019).
- [51] M. Delfan Azari, S. Yamada, T. Morinaga, H. Nagakura, S. Furusawa, A. Harada, H. Okawa, W. Iwakami, and K. Sumiyoshi, Fast collective neutrino oscillations inside the neutrino sphere in core-collapse supernovae, *Physical Review D* **101**, 023018 (2020).
- [52] R. Glas, H. Thomas Janka, F. Capozzi, M. Sen, B. Dasgupta, A. Mirizzi, and G. Sigl, Fast neutrino flavor instability in the neutron-star convection layer of three-dimensional supernova models, *Physical Review D* **101**, 063001 (2020).
- [53] T. Morinaga, H. Nagakura, C. Kato, and S. Yamada, Fast neutrino-flavor conversion in the preshock region of core-collapse supernovae, *Physical Review Research* **2**, 012046(R) (2020).
- [54] G. Mangano, A. Mirizzi, and N. Saviano, Damping the neutrino flavor pendulum by breaking homogeneity, *Phys. Rev. D* **89**, 073017 (2014), arXiv:1403.1892 [hep-ph].
- [55] S. Abbar, Turbulence Fingerprint on Collective Oscillations of Supernova Neutrinos, *Phys. Rev. D* **103**, 045014 (2021), arXiv:2007.13655 [astro-ph.HE].
- [56] G. Sigl, Simulations of Fast Neutrino Flavor Conversions with Interactions in Inhomogeneous Media, arXiv e-prints, arXiv:2109.00091 (2021), arXiv:2109.00091 [hep-ph].
- [57] H. Duan, G. M. Fuller, and J. Carlson, Simulating nonlinear neutrino flavor evolution, *Computational Science and Discovery* **1**, 015007 (2008), arXiv:0803.3650 [astro-ph].
- [58] S. Sarikas, D. de Sousa Seixas, and G. Raffelt, Spurious instabilities in multiangle simulations of collective flavor conversion, *Phys. Rev. D* **86**, 125020 (2012), arXiv:1210.4557 [hep-ph].
- [59] W. Iwakami, H. Okawa, H. Nagakura, A. Harada, S. Furusawa, K. Sumiyoshi, H. Matsufuru, and S. Yamada, Simulations of the Early Postbounce Phase of Core-collapse Supernovae in Three-dimensional Space with Full Boltzmann Neutrino Transport, *Astrophys. J.* **903**, 82 (2020), arXiv:2004.02091 [astro-ph.HE].
- [60] Y.-F. Jiang, J. M. Stone, and S. W. Davis, An Algorithm for Radiation Magnetohydrodynamics Based on Solving the Time-dependent Transfer Equation, *The Astrophysical Journal Supplement* **213**, 7 (2014), arXiv:1403.6126 [astro-ph.IM].
- [61] N. P. Cimerman, R. Kuiper, and C. W. Ormel, Hydrodynamics of embedded planetsâ€™ first atmospheres â€“ III. The role of radiation transport for super-Earth planets, *Monthly Notices of the Royal Astronomical Society* **471**, 4662 (2017).
- [62] G. Birindelli, J.-L. Feugeas, J. Caron, B. Dubroca, G. Kantor, J. Page, T. Pichard, V. Tikhonchuk, and P. Nicola, High performance modelling of the transport of energetic particles for photon radiotherapy, *Phys-*

- ica Medica **42**, 305 (2017).
- [63] P. F. Hopkins and M. Y. GrudiÄš, Numerical problems in coupling photon momentum (radiation pressure) to gas, *Monthly Notices of the Royal Astronomical Society* **483**, 4187 (2019).
- [64] H. Bloch, P. Tremblin, M. González, T. Padioleau, and E. Audit, A high-performance and portable asymptotic preserving radiation hydrodynamics code with the M1 model, *Astronomy & Astrophysics* **646**, A123 (2021), publisher: EDP Sciences.
- [65] J. D. Melon Fuksman, H. Klahr, M. Flock, and A. Mignone, A Two-moment Radiation Hydrodynamics Scheme Applicable to Simulations of Planet Formation in Circumstellar Disks, *The Astrophysical Journal* **906**, 78 (2021), arXiv:2005.01785 [astro-ph.EP].
- [66] A. Vlasenko, G. M. Fuller, and V. Cirigliano, Neutrino quantum kinetics, *Physical Review D* **89**, 105004 (2014).
- [67] C. Volpe, Neutrino quantum kinetic equations, *International Journal of Modern Physics E* **24**, 1541009 (2015).
- [68] D. N. Blaschke and V. Cirigliano, Neutrino quantum kinetic equations: The collision term, *Physical Review D* **94**, 033009 (2016).
- [69] P. Strack and A. Burrows, Generalized Boltzmann formalism for oscillating neutrinos, *Physical Review D* **71**, 093004 (2005), publisher: American Physical Society.
- [70] H. Duan and S. Shalgar, Multipole expansion method for supernova neutrino oscillations, *JCAP* **2014** (10), 084, arXiv:1407.7861 [hep-ph].
- [71] S. A. Richers, G. C. McLaughlin, J. P. Kneller, and A. Vlasenko, Neutrino quantum kinetics in compact objects, *Physical Review D* **99**, 123014 (2019).
- [72] L. Johns, H. Nagakura, G. M. Fuller, and A. Burrows, Fast oscillations, collisionless relaxation, and spurious evolution of supernova neutrino flavor, *Physical Review D* **102**, 103017 (2020).
- [73] Y. Zhang and A. Burrows, Transport equations for oscillating neutrinos, *Physical Review D* **88**, 105009 (2013).
- [74] K. S. Thorne, Relativistic radiative transfer - Moment formalisms, *Monthly Notices of the Royal Astronomical Society* **194**, 439 (1981).
- [75] J. M. Smit, L. J. van den Horn, and S. A. Bludman, Closure in flux-limited neutrino diffusion and two-moment transport, *Astronomy and Astrophysics* **356**, 559 (2000).
- [76] E. M. Murchikova, E. Abdikamalov, and T. Urbatsch, Analytic closures for M1 neutrino transport, *Monthly Notices of the Royal Astronomical Society* **469**, 1725 (2017).
- [77] J. C. Hayes and M. L. Norman, Beyond Flux-limited Diffusion: Parallel Algorithms for Multidimensional Radiation Hydrodynamics, *The Astrophysical Journal Supplement Series* **147**, 197 (2003), publisher: American Astronomical Society.
- [78] I. Hubeny and A. Burrows, A New Algorithm for Two-Dimensional Transport for Astrophysical Simulations. I. General Formulation and Tests for the One-Dimensional Spherical Case, *The Astrophysical Journal* **659**, 1458 (2007), publisher: American Astronomical Society.
- [79] B. Dasgupta, A. Dighe, A. Mirizzi, and G. Raffelt, Collective neutrino oscillations in nonspherical geometry, *Phys. Rev. D* **78**, 033014 (2008), arXiv:0805.3300 [hep-ph].
- [80] A. Mirizzi and P. D. Serpico, Instability in the Dense Supernova Neutrino Gas with Flavor-Dependent Angular Distributions, *Physical Review Letters* **108**, 231102 (2012), publisher: American Physical Society.
- [81] M. T. Keil, G. G. Raffelt, and H. Janka, Monte Carlo Study of Supernova Neutrino Spectra Formation, *The Astrophysical Journal* **590**, 971 (2003).
- [82] I. Tamborra and S. Shalgar, New Developments in Flavor Evolution of a Dense Neutrino Gas, arXiv e-prints, arXiv:2011.01948 (2020), arXiv:2011.01948 [astro-ph.HE].
- [83] H. Duan, G. M. Fuller, J. Carlson, and Y.-Z. Qian, Neutrino Mass Hierarchy and Stepwise Spectral Swapping of Supernova Neutrino Flavors, *Physical Review Letters* **99**, 241802 (2007), publisher: American Physical Society.
- [84] B. Dasgupta, A. Dighe, G. G. Raffelt, and A. Y. Smirnov, Multiple Spectral Splits of Supernova Neutrinos, *Physical Review Letters* **103**, 051105 (2009), publisher: American Physical Society.
- [85] T. Fischer, S. C. Whitehouse, A. Mezzacappa, F. K. Thielemann, and M. Liebendörfer, Proton-neutron star evolution and the neutrino-driven wind in general relativistic neutrino radiation hydrodynamics simulations, *Astronomy & Astrophysics* **517**, A80 (2010), arXiv:0908.1871 [astro-ph.HE].
- [86] H. Duan, G. M. Fuller, and Y.-Z. Qian, Collective neutrino flavor transformation in supernovae, *Physical Review D* **74**, 123004 (2006), publisher: American Physical Society.
- [87] B. Dasgupta, A. Dighe, G. G. Raffelt, and A. Y. Smirnov, Multiple spectral splits of supernova neutrinos, *Phys. Rev. Lett.* **103**, 051105 (2009).
- [88] J. D. Hunter, Matplotlib: A 2d graphics environment, *Computing in Science Engineering* **9**, 90 (2007).
- [89] S. van der Walt, S. C. Colbert, and G. Varoquaux, The numpy array: A structure for efficient numerical computation, *Computing in Science Engineering* **13**, 22 (2011).
- [90] E. Jones, T. Oliphant, P. Peterson, *et al.*, SciPy: Open source scientific tools for Python (2001), [Online; accessed *today*].
- [91] H. Duan, G. M. Fuller, J. Carlson, and Y.-Z. Qian, Coherent Development of Neutrino Flavor in the Supernova Environment, *Physical Review Letters* **97**, 241101 (2006), publisher: American Physical Society.
- [92] H. Duan, G. M. Fuller, J. Carlson, and Y.-Z. Qian, Simulation of coherent non-linear neutrino flavor transformation in the supernova environment. i: Correlated neutrino trajectories, *Phys. Rev.* **74**, 105014 (2006), arXiv:astro-ph/0606616.
- [93] B. D. Keister, Numerical and physical stability of supernova neutrino flavor evolution, *Physica Scripta* **90**, 088008 (2015), arXiv:1408.4729 [astro-ph.HE].
- [94] S. A. Richers, G. C. McLaughlin, J. P. Kneller, and A. Vlasenko, Neutrino quantum kinetics in compact objects, *Phys. Rev. D* **99**, 123014 (2019), arXiv:1903.00022 [astro-ph.HE].